Progress In Electromagnetics Research, PIER 104, 85–97, 2010

A NOVEL HYBRID AIPO-MOM TECHNIQUE FOR JET ENGINE MODULATION ANALYSIS

H. Lim and N. H. Myung

Department of Electrical Engineering
Korea Advanced Institute of Science and Technology (KAIST)
335 Gwahangno, Yuseong-gu, Daejeon 305-701, Korea

Abstract—A novel hybrid adaptive iterative physical optics-method of moments (AIPO-MoM) technique is presented for the electromagnetic analysis of jet engine structures that are both electrically large and complex in both stationary and dynamic cases. In this technique, the AIPO method is used to analyze the smooth inlet region, and the MoM method is used to analyze the electrically complex compressor region, including blades and a hub. It is efficient and accurate by virtue of combining the respective merits of both methods. In the dynamic case, a concept for modified impedance equation is proposed to reduce computational load. Numerical results are presented and verified through comparison with Mode-FDTD and measured and commercial simulation packages results.

1. INTRODUCTION

The analysis of wave scattering from fighters is one of the most challenging research subjects in the area of electromagnetic studies. It has been found that, among various factors contributing to RCS of a fighter, wave scattering from a jet engine inlet is one of the most critical. Based on this, numerous studies have been carried out to analyze wave scattering from these structures. In the early stages of research, analytic methods were applied to very simple canonical structures. More recently, however, a variety of numerical algorithms have been used by virtue of outstanding improvement of computer performance. These algorithms include mode analysis, high frequency (HF) methods, and hybrid methods. The mode analysis technique gives precise results only to very simple canonical structures. The

Corresponding author: H. Lim (limho@kaist.ac.kr).

HF methods such as the geometrical optics (GO), uniform theory of diffraction (UTD), physical optics (PO), and physical theory of diffraction (PTD) are applicable limitedly to electrically large and smooth structures. In addition, low frequency (LF) methods such as finite element method (FEM), method of moment (MoM), and finite difference time domain (FDTD) have been utilized, but they are limited to electrically small structures. Consequently, hybrid methods incorporating two kinds of methods such as Mode-FEM [1], Mode-FDTD [2], GRE-FDTD [2], and IPO-FDTD [2, 3] methods have recently been used to analyze wave scattering from jet engine structures that are both electrically large and complex.

Despite the abundance of methods developed to date, as outlined above, there has been scarce research on jet engine modulation (JEM) analyses, that is, analyses under the situation where blades connected to a shaft are rotated. In particular, very little research in this regard has been done with hybrid methods. Only a few studies involving JEM analyses, such as a mode based analysis technique that makes use of the overlapping symmetries between the modal inlet fields and the engine face, can be found in the open literature [4].

In this paper, the adaptive iterative physical optics (AIPO) method is used for the HF region, and the transmitted fields are calculated at the virtual surface, which is the interface between the HF and LF regions. These fields are used as sources of the MoM method, which analyzes the LF region and calculates scattered fields at the virtual surface. Finally, a monostatic RCS is calculated from both the transmitted and scattered fields using the generalized reciprocity theorem. Analysis of the situation where blades connected to a shaft are rotated is efficiently performed by virtue of the proposed modified impedance equation.

2. THE HYBRID AIPO-MOM TECHNIQUE

2.1. Structure Description

The jet engine models can be decomposed into an inlet as a HF region and a compressor as a LF region to implement the domain decomposition method (DDM) [5–9] which is useful to solve electrically large scale problems, as illustrated in Fig. 1. The plane C_0 indicates an aperture where an incident plane wave enters, and the plane C_1 is a virtual interface that separates the HF and LF regions. The wave scattering is concerned to be from the inner surface, not from the outer surface of the model. The analysis procedure is shown in Fig. 2, and details of the procedure are presented in the following sections.

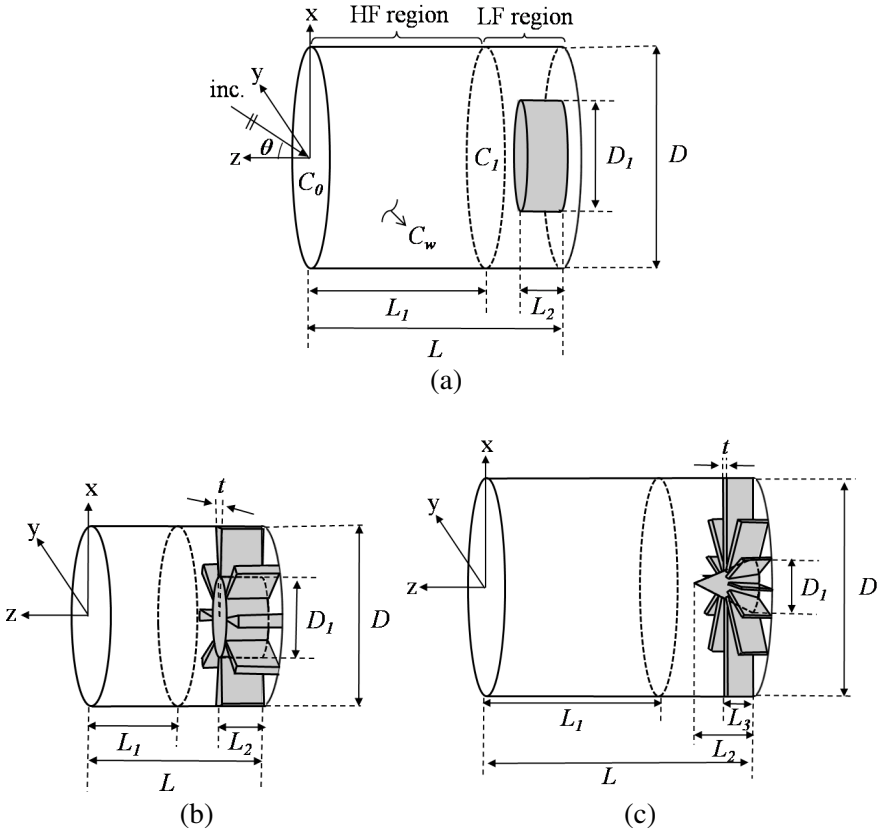

Figure 1. Jet engine models. (a) Model A ($L = 10\lambda$, $L_1 = 8\lambda$, $L_2 = 1\lambda$, $D = 8\lambda$, $D_1 = 4\lambda$) and (b) Model B ($L = 6\lambda$, $L_1 = 3\lambda$, $L_2 = 2\lambda$, $D = 6\lambda$, $D_1 = 3\lambda$, $t = 5°$) and (c) Model C ($L = 11\lambda$, $L_1 = 8\lambda$, $L_2 = 2\lambda$, $L_3 = 1\lambda$, $D = 8\lambda$, $D_1 = 2\lambda$, $t = 0.1\lambda$).

2.2. AIPO

The transmitted fields at C_1 are determined by the AIPO in the HF region, which is modeled by square flat facets. The density of the AIPO region is determined by considering accuracy, computation time and memory limits (typically $8 \sim 10$ facets per wavelength to fitness). The first step to implement the AIPO is to find initial currents at the center point of every facet on the illuminated inner sidewall using the PO approximation by (1).

$$\bar{J}_0 = 2\hat{n}_w \times \bar{H}^i \tag{1}$$

where $\hat{n}_w$ is a unit vector normal to the inner sidewall C_w.

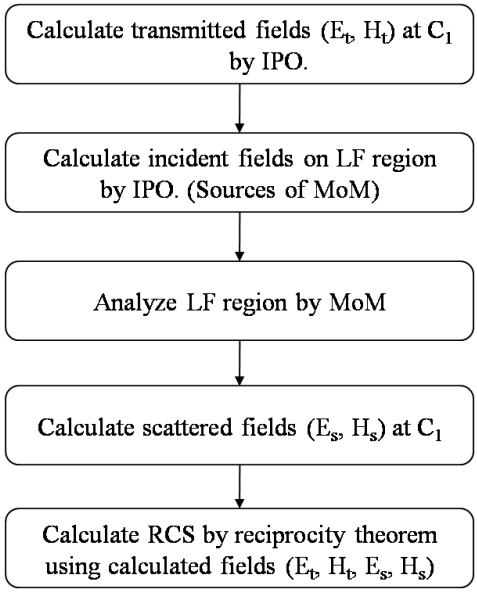

Figure 2. AIPO-MoM analysis procedure.

The current on the inner sidewall is iteratively calculated [10] until convergence is reached using ray tracing and/or the change rate of current [3] by (2).

$$\bar{J}_n\left(\bar{r}_c\right) = \bar{J}_0 + 2\hat{n}_w \times \left[\iint_{C_w} \bar{J}_{n-1}\left(\bar{r}'_c\right) \times \nabla G_0\left(\bar{r}_c - \bar{r}'_c\right) ds\right], \qquad (2)$$

where

$$\nabla G_0\left(\bar{r}_c - \bar{r}'_c\right) = \hat{R}\left(jk_0R + 1\right)\frac{e^{-jk_0R}}{4\pi R^2},$$
$$R = \left|\bar{r}_c - \bar{r}'_c\right|, \quad \hat{R} = \frac{\left(\bar{r}_c - \bar{r}'_c\right)}{\left|\bar{r}_c - \bar{r}'_c\right|}, \quad n = 1, 2, \ldots, N$$

where $\bar{r}_c$ are center points of facets on C_w, and $\nabla G_0\left(\bar{r}_c - \bar{r}'_c\right)$ is a gradient of Green's function.

The method to use ray tracing to determine the number of iterations is as follows. The incident field is divided into several ray tubes. The path of each tube is traced until it reaches C_1, and the number of reflections of each tube is calculated. The highest percentage number among them is determined as the number of iterations. The method to use the change rate of current is as follows. The amount of energy proportional to the current energy of all patches is defined

as (3).

$$Energy\left(J_n\right) \equiv \sum_{all\ patches} \sqrt{\left[\left|J_{nx}\right|^2 + \left|J_{ny}\right|^2 + \left|J_{nz}\right|^2\right]} \tag{3}$$

The change rate of the amount of energy is defined as (4).

$$Change\ rate\left(n\right) \equiv \left|\frac{Energy\left(J_n\right) - Energy\left(J_{n-1}\right)}{Energy\left(J_{n-1}\right)}\right| \times 100\left(\%\right) \tag{4}$$

The number of iterations is determined when the change rate is below a certain threshold (typically $3 \sim 5\%$ to fitness). The stable current is calculated using these two methods. Thereafter, we can calculate the transmitted fields at the center of every facet on C_1 by (5) and (6).

$$\bar{H}\left(\bar{r}_{c_1}\right) = \iint_{C_w} \bar{J}_N\left(\bar{r}_c\right) \times \nabla G_0\left(\bar{r}_{c_1} - \bar{r}_c\right) ds + \bar{H}^i\left(\bar{r}_{c_1}\right) \tag{5}$$

$$\bar{E}\left(\bar{r}_{c_1}\right) = \frac{\eta}{jk_0}\nabla \times \iint_{C_w} \bar{J}_N\left(\bar{r}_c\right) \times \nabla G_0\left(\bar{r}_{c_1} - \bar{r}_c\right) ds + \bar{E}^i\left(\bar{r}_{c_1}\right) \tag{6}$$

where $\bar{r}_{c_1}$ are center points of facets on C_1.

2.3. MoM

The scattered fields at C_1 are determined by the MoM in the LF region, which is modeled by triangular flat facets. The density of the MoM region is determined by considering accuracy, computation time and memory limits (typically $8 \sim 10$ facets per wavelength to fitness). The Rao-Wilton-Glisson (RWG) basis function [11] is used. RWG edge elements including geometrical data (edge node numbers, edge lengths, triangle areas, triangle centers, position vectors, etc.) are determined for constructing an impedance matrix. The impedance matrix of the electric field integral equation (EFIE) is then determined by (7), and the surface current density is determined using the impedance equation, given as (8) [12].

$$Z_{mn} = l_m \left[j\omega\left(\frac{\bar{A}^+_{mn} \cdot \bar{\rho}^{c+}_m}{2} + \frac{\bar{A}^-_{mn} \cdot \bar{\rho}^{c-}_m}{2}\right) + \Phi^-_{mn} - \Phi^+_{mn}\right], \tag{7}$$

where $m, n = 1, 2, \ldots, M$,

$$\bar{A}^{\pm}_{mn} = \frac{\mu}{4\pi}\left[\frac{l_n}{2A^+_n}\int_{T^+_n} \bar{\rho}^+_m\left(\bar{r}'\right) g^{\pm}_m\left(\bar{r}'\right) dS' + \frac{l_n}{2A^-_n}\int_{T^-_n} \bar{\rho}^-_m\left(\bar{r}'\right) g^{\pm}_m\left(\bar{r}'\right) dS'\right],$$

$$\Phi^{\pm}_{mn} = \frac{1}{4\pi j\omega\epsilon}\left[\frac{l_n}{A^+_n}\int_{T^+_n} g^{\pm}_m\left(\bar{r}'\right) dS' - \frac{l_n}{A^-_n}\int_{T^-_n} g^{\pm}_m\left(\bar{r}'\right) dS'\right],$$

$$\bar{\rho}^{c+}_m = \bar{r}^{c+}_m - \bar{\nu}^+_m, \quad \rho^{c-}_m = -\bar{r}^{c-}_m + \bar{\nu}^-_m, \quad g^{\pm}_m\left(\bar{r}'\right) = \frac{e^{-jk\left|\bar{r}^{c\pm}_m - \bar{r}'\right|}}{\left|\bar{r}^{c\pm}_m - \bar{r}'\right|}$$

$$\mathbf{Z} \cdot \mathbf{I} = \mathbf{V}, \tag{8}$$

where

$$V_m = l_m \left(\frac{\bar{E}_m^+ \cdot \bar{\rho}_m^{c+}}{2} + \frac{\bar{E}_m^- \cdot \bar{\rho}_m^{c-}}{2} \right), \; \bar{E}_m^{\pm} = \bar{E}^{inc} \left(\bar{r}_m^{c\pm} \right), \; m = 1, 2, \ldots, M$$

where m and n are the mth and nth edge elements, respectively. l_m is the length of the mth edge element, $\bar{\rho}_m^{c\pm}$ are vectors between the free vertex point, $\bar{\nu}_m^{\pm}$, and the centroid point, $\bar{r}_m^{c\pm}$, of the two triangles $T_m^{\pm}$ of the mth edge element, respectively, and $\bar{E}^{inc}$ is the electric field of an incident electromagnetic signal. $\mathbf{Z}$ is the impedance matrix and $\mathbf{I}$ and $\mathbf{V}$ are the current and voltage vectors, respectively.

2.4. Connection between AIPO and MoM

The most important aspect in hybrid methods is coupling between HF and LF methods. The incident field at the entrance of the jet engine propagates through the HF region, C_1, and the LF region, in turn, and after reflecting, propagates back through C_1. The jet engine structure with the physical characteristics of these propagations can be separated in the HF and LF regions, and each region can be analyzed independently using the generalized reciprocity theorem [13]. Therefore, the AIPO and the MoM are connected through a single calculation from stable currents on the HF region to fields on the LF region, as is the case with other hybrid methods [2, 3]. That is, in the AIPO-MoM, we exported center points of triangle patches in the LF region, and then calculated electric fields at those positions by the AIPO. Those fields are sources of the MoM. Scattered fields on C_1 are calculated using the dipole model [14] by (9), (10).

$$\bar{H}\left(\bar{r}_{c_1}\right) = \sum_{m=1}^{M} \bar{H}_m \left(\bar{r}_{c_1} - \frac{1}{2}\left(\bar{r}_m^{c+} + \bar{r}_m^{c-} \right) \right) \tag{9}$$

$$\bar{E}\left(\bar{r}_{c_1}\right) = \sum_{m=1}^{M} \bar{E}_m \left(\bar{r}_{c_1} - \frac{1}{2}\left(\bar{r}_m^{c+} + \bar{r}_m^{c-} \right) \right), \tag{10}$$

where

$$\bar{H}\left(\bar{r}\right) = \frac{jk}{4\pi}\left(\bar{m} \times \bar{r}\right) C e^{-jkr}, C = \frac{1}{r^2}\left[1 + \frac{1}{jkr}\right],$$

$$\bar{E}\left(\bar{r}\right) = \frac{\eta}{4\pi}\left(\left(\bar{M} - \bar{m}\right)\left[\frac{jk}{r} + C\right] + 2\bar{M}C \right) e^{-jkr},$$

$$\bar{m} = \int_{T_m^+ + T_m^-} I_m \bar{f}_m\left(\bar{r}\right) dS = l_m I_m \left(\bar{r}_m^{c-} - \bar{r}_m^{c+} \right),$$

$$\bar{M} = \frac{(\bar{r} \cdot \bar{m})\,\bar{r}}{r^2}$$

where $\bar{m}$ is a dipole moment, $\bar{f}_m(\bar{r})$ is a RWG basis function, and I_m is a surface current coefficient corresponding to the mth element.

2.5. RCS Calculation Using the Generalized Reciprocity Theorem

The monostatic RCS can be obtained by the generalized reciprocity theorem in jet engine structure cases [2, 13, 15, 16]. With the theorem, we can eliminate the computational load, i.e., the reverse repetitive calculation by the AIPO from fields on C_1 to C_0. For the structure in Fig. 1, we can represent the theorem by Equation (11) as [13].

$$\bar{P}_t \cdot \bar{E}_s(\bar{r}) = \iint_{C_1} \left(\bar{E}_s \times \bar{H}_t - \bar{E}_t \times \bar{H}_s\right) \cdot d\bar{S} \tag{11}$$

where $\bar{P}_t$ is the vector of a test current source, $\bar{r}$ is the observation point outside the scatterer, $(\bar{E}_t, \bar{H}_t)$ are the transmitted fields at C_1 calculated by the AIPO, and $(\bar{E}_s, \bar{H}_s)$ are the scattered fields at C_1 calculated by the MoM.

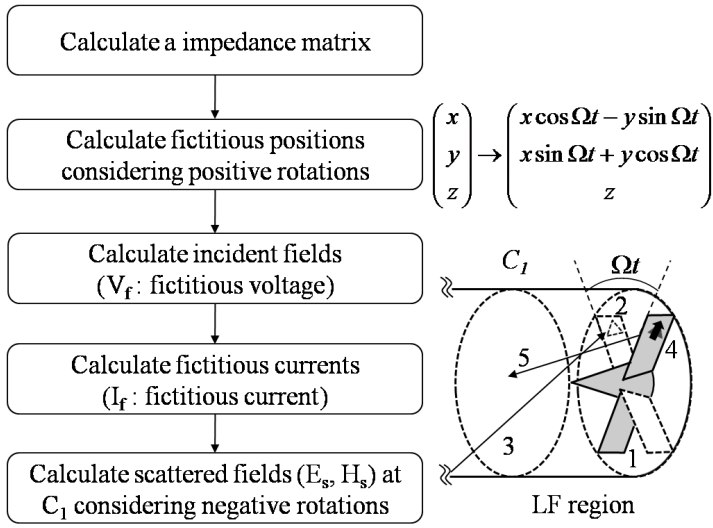

Figure 3. JEM analysis procedure using AIPO-MoM.

2.6. Jet Engine Modulation Calculation using AIPO-MoM

When blades connected to a shaft are rotated, mesh information of the blades for the MoM calculation changes. There are numerous computations to calculate impedance matrices of all positions individually. The authors have developed an alternative technique, however, to reduce the computational load using modified impedance equations. The analysis procedure of JEM using the AIPO-MoM is described in Fig. 3. The same stages as the stationary case (1 and 5 stages) in Fig. 2 are omitted. The revised stages with the stationary case (2, 3, and 4 stages) are described in detail as 5 steps. In the technique using the modified impedance equations, the LF region is modeled only once. The impedance matrix is also calculated only once, and then repeatedly used, because the relative positions of meshes do not change when the blades connected to the shaft are rotated. The fictitious voltages are determined considering positive rotations with original position information when the blades connected to the shaft are rotated. The fictitious currents are determined using the impedance matrix and the fictitious voltages via Equation (12).

$$\mathbf{Z} \cdot \mathbf{I_f} = \mathbf{V_f}, \tag{12}$$

where

$$V_{f,m} = l_m \left(\frac{\bar{E}^{+}_{f,m} \cdot \bar{\rho}^{c+}_{f,m}}{2} + \frac{\bar{E}^{-}_{f,m} \cdot \bar{\rho}^{c-}_{f,m}}{2} \right), \quad \bar{E}^{\pm}_{f,m} = \bar{E}^{inc}\left(\bar{r}^{c\pm}_{f,m}\right),$$

$$m = 1, 2, \ldots, M$$

where $\mathbf{Z}$ is the impedance matrix and $\mathbf{I_f}$ and $\mathbf{V_f}$ are the fictitious current and voltage vectors, respectively.

Scattered fields on C_1 are determined considering negative rotations with the original position information, because the fictitious currents are located at the original positions.

3. NUMERICAL RESULTS

The proposed hybrid AIPO-MoM technique for the structure in Fig. 1 is simulated and verified through comparison with other data [2, 17]. The normalized mean square error (nMSE) is defined to examine the accuracy as (13).

$$nMSE \equiv \frac{\sum_{n=1}^{N} |RCS_n^p - RCS_n^r|^2}{\sum_{n=1}^{N} |RCS_n^r|^2} \tag{13}$$

where RCS_n^p and RCS_n^r are the linear scaled RCS calculated by the proposed AIPO-MoM and referenced method at the nth sample, respectively.

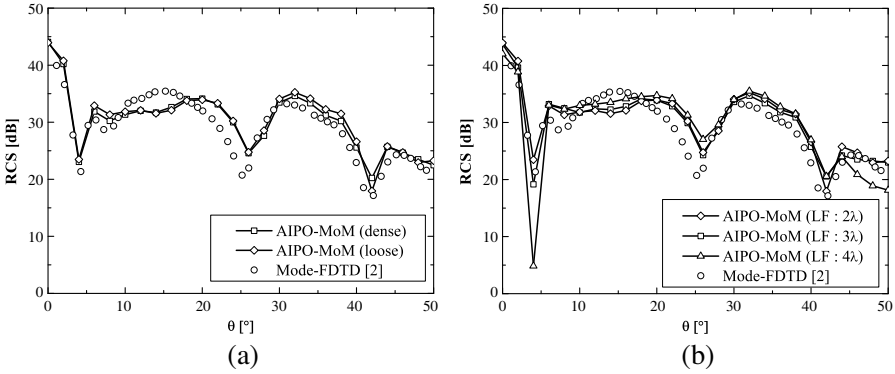

Figure 4. Monostatic RCS results of model A (θ-θ) with (a) different densities of mesh modeling and (b) different positions of C_1 plane.

Table 1. The nMSE values for different densities of mesh modeling and different positions of C_1 plane in Fig. 4.

dense	loose	LF: 2λ	LF: 3λ	LF: 4λ
0.453	0.467	0.467	0.306	0.069

Model A is an open-ended circular cavity (OECC) with a disk type hub and is analyzed in a stationary case. The monostatic RCS results with different densities of mesh modeling and different positions of C_1 plane are compared with the results of Mode-FDTD, as seen in Fig. 4.

Table 1 shows the nMSE values for different densities of mesh modeling and different positions of C_1 plane in Fig. 4. In Table 1, dense means that the densities of the HF and LF regions are 10 facets and 8 facets per wavelength, and loose means that the densities of the HF and LF regions are 4 facets and 5 facets per wavelength, respectively. It can be seen that the accuracy slightly increases as the density increases, and the accuracy increases as the LF region increases.

Model B is an OECC with a disk type hub and 8 thin fan-shaped blades, and is analyzed in both stationary and dynamic cases. The monostatic RCS results of AIPO-MoM for the stationary case with different densities of mesh modeling are compared with the measured results of Anastassiu, as seen in Fig. 5.

Table 2 shows the nMSE values for different densities of mesh modeling in Fig. 5. In Table 2, dense means that the densities of the HF and LF regions are 10 facets and 7 facets per wavelength, and loose means that the densities of the HF and LF regions are 4 facets and $4 \sim 6$ facets per wavelength, respectively. It can be seen that the accuracy increases as the density increases.

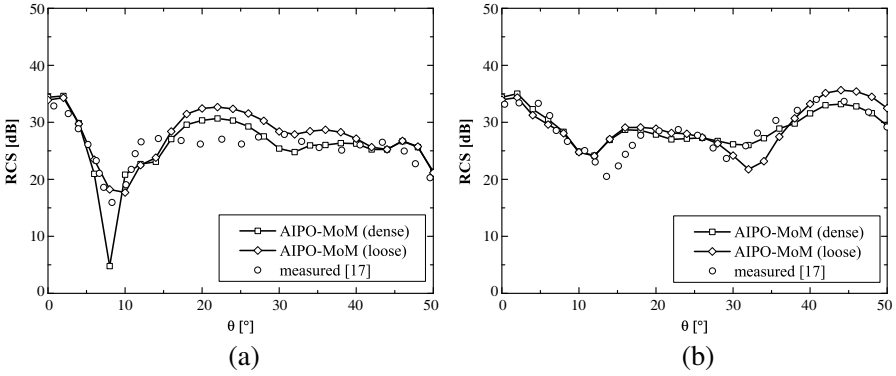

Figure 5. Monostatic RCS results of model B with different densities of mesh modeling. (a) θ-θ and (b) ϕ-ϕ.

Table 2. The nMSE values for different densities of mesh modeling in Fig. 5.

	dense	loose
θ-θ	0.368	0.826
ϕ-ϕ	0.083	0.230

Table 3. The normalized CPU times in each of the steps of Fig. 2 and Fig. 3 corresponding to the model B with the dense density. (%)

	stage 1	stage 2	stage 3	stage 4	stage 5	total
Fig. 2 (stationary)	8.3	7.0	74.4	9.9	0.4	100
	step 1	step 2	step 3	step 4	step 5	total
Fig. 3 (dynamic)	64.4	0.1	7.0	9.9	9.9	91.3

Table 3 shows the CPU times to show percentage of time spending in each of the steps of Fig. 2 and Fig. 3 corresponding to the model B with the dense density. The times are normalized to the CPU time of total computation. In dynamic case, the same stages as the stationary case (1 and 5 stages) are omitted. The revised stages with the stationary case (2, 3, and 4 stages) are described in detail as 5 steps, and the CPU time corresponding to step 1 is reduced in each time sample, because the impedance matrix is calculated only once.

The result of AIPO-MoM for the dynamic case agrees well with the result of MoM from commercial simulation packages, FEKO, and a period of 45 degrees due to 8 blades is observed, as shown in Fig. 6(a).

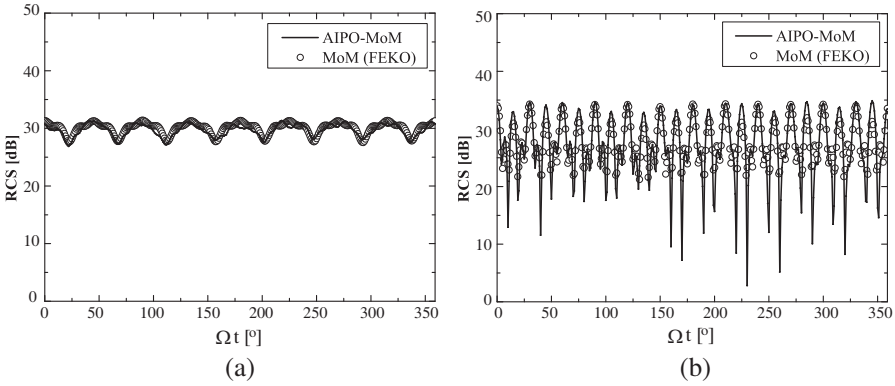

Figure 6. Monostatic RCS results when blades connected to a shaft are rotated. (a) Model B (ϕ-ϕ, $\theta = 38°$) and (b) Model C (ϕ-ϕ, $\theta = 38°$).

Model C is an OECC with a conical type hub and 12 thin straight blades and is analyzed in a dynamic case. The result of AIPO-MoM agrees well with the result of MoM from FEKO and a period of 30 degrees due to 12 blades is observed, as seen in Fig. 6(b). In this case, fluctuations are much more complicated than in the former case from the viewpoint of the number of fluctuations and the change rate, due to a much sharper hub and more blades.

4. CONCLUSION

We applied a novel hybrid AIPO-MoM technique to a jet engine scattering analysis for the first time. A simple connection procedure between AIPO and MoM was suggested, and the analysis procedures for both stationary and dynamic cases were described in detail. A technique using modified impedance equations was proposed for the case when blades connected to a shaft are rotated. It was shown that the computational load could be reduced. Numerical results demonstrate the reliability of the proposed technique. This technique can be useful for jet engine structures with a non-canonical inlet structure and more complicated protrusions due to the advantages of the AIPO and MoM, respectively, and shows remarkable strength in JEM analysis by virtue of the proposed modified impedance equation.

ACKNOWLEDGMENT

This research was supported by the ADD (Agency for Defense Development), Korea, through the RDRC (Radiowave Detection Research Center) at KAIST (Korea Advanced Institute of Science and Technology).

REFERENCES

1. Ross, D. C., J. L. Volakis, and H. T. Anastassiu, "Hybrid finite element-modal analysis of jet engine inlet scattering," *IEEE Trans. Antennas Propag.*, Vol. 43, No. 3, 277–285, 1995.
2. Chia, T. T., R. J. Burkholder, and R. Lee, "The application of FDTD in hybrid methods for cavity scattering analysis," *IEEE Trans. Antennas Propag.*, Vol. 43, No. 10, 1082–1090, 1995.
3. Choi, S. H., D. W. Seo, and N. H. Myung, "Scattering analysis of open-ended cavity with inner object," *Journal of Electromagnetic Waves and Applications*, Vol. 21, No. 12, 1689–1702, 2007.
4. Ross, D. C., J. L. Volakis, and H. T. Anastassiu, "Efficient computation of radar scattering modulation from jet engines," *Radio Sci.*, Vol. 31, No. 4, 991–997, 1996.
5. Stupfel, B. and B. Després, "A domain decomposition method for the solution of large electromagnetic scattering problems," *Journal of Electromagnetic Waves and Applications*, Vol. 13, No. 11, 1553–1568, 1999.
6. Sharkawy, M. A., V. Demir, and A. Z. Elsherbeni, "The iterative multi-region algorithm using a hybrid finite difference frequency domain and method of moments techniques," *Progress In Electromagneitcs Research*, PIER 57, 19–32, 2006.
7. Ozgun, O. and M. Kuzuoglu, "Finite element analysis of electromagnetic scattering problems via iterative leap-field domain decomposition method," *Journal of Electromagnetic Waves and Applications*, Vol. 22, No. 2–3, 251–266, 2008.
8. Duan, Y., S. J. Lai, and T. Huang, "Coupling projection domain decomposition method and meshless collocation method using radial basis functions in electromagnetics," *Progress In Electromagnetics Research Letters*, Vol. 5, 1–12, 2008.
9. Martini, E., G. Carli, and S. Maci, "A domain decomposition method based on a generalized scattering matrix formalism and a complex source expansion," *Progress In Electromagnetics Research B*, Vol. 19, 445–473, 2010.
10. Obelleiro-Basteiro, F., J. L. Rodriguez, and R. J. Burkholder,

"An iterative physical optics approach for analyzing the electromagnetic scattering by large open-ended cavities," *IEEE Trans. Antennas Propag.*, Vol. 43, No. 4, 356–361, 1995.

11. Rao, S. M., D. R. Wilton, and A. W. Glisson, "Electromagnetic scattering by surfaces of arbitrary shape," *IEEE Trans. Antennas Propag.*, Vol. 30, No. 3, 409–418, 1982.
12. Makarov, S. N., *Antenna and EM Modeling with Matlab*, Wiley-Interscience, New York, 2002.
13. Pathak, P. H. and R. J. Burkholder, "A reciprocity formulation for the EM scattering by an obstacle within a large open cavity," *IEEE Trans. Microwave Theory Techniques*, Vol. 41, No. 4, 702–707, 1993.
14. Leat, C. J., N. V. Shuley, and G. F. Stickley, "Triangular-patch model of bowtie antennas: Validation against Brown and Woodward," *IEE Proc. Microw. Antennas Propag.*, Vol. 145, No. 6, 465–470, 1998.
15. Rousseau, P. R. and R. J. Burkholder, "A hybrid approach for calculating the scattering from obstacles within large, open cavities," *IEEE Trans. Antennas Propag.*, Vol. 43, No. 10, 1068–1075, 1995.
16. Obelleiro, F., J. Campos-Nino, J. L. Rodriguez, and A. G. Pino, "A segmented approach for computing the electromagnetic scattering of large and deep cavities," *Progress In Electromagnetics Research*, PIER 19, 129–145, 1998.
17. Anastassiu, H. T., J. L. Volakis, D. C. Ross, and D. Andersh, "Electromagnetic scattering from simple jet engine models," *IEEE Trans. Antennas Propag.*, Vol. 44, No. 3, 420–421, 1996.